

# SDSS IV MANGA - ROTATION VELOCITY LAGS IN THE EXTRAPLANAR IONIZED GAS FROM MANGA OBSERVATIONS OF EDGE-ON GALAXIES

BIZYAEV, D.<sup>1,2,3</sup>, WALTERBOS, R. A. M.<sup>4</sup>, YOACHIM, P.<sup>5</sup>, RIFFEL, R. A.<sup>6,7</sup>, FERNÁNDEZ-TRINCADO, J. G.<sup>8</sup>, PAN, K.<sup>1</sup>, DIAMOND-STANIC, A. M.<sup>9,10</sup>, JONES, A.<sup>11</sup>, THOMAS, D.<sup>12</sup>, CLEARY, J.<sup>13</sup>, BRINKMANN, J.<sup>1</sup>

<sup>1</sup>Apache Point Observatory and New Mexico State University, Sunspot, NM, 88349, USA

<sup>2</sup>Sternberg Astronomical Institute, Moscow State University, Moscow, Russia

<sup>3</sup>Special Astrophysical Observatory of the Russian AS, 369167, Nizhnij Arkhyz, Russia

<sup>4</sup>Department of Astronomy, New Mexico State University, Las Cruces, NM, 88003, USA

<sup>5</sup>Department of Astronomy, University of Washington, Seattle, WA, 98195, USA

<sup>6</sup>Departamento de Física, CCNE, Universidade Federal de Santa Maria, Av. Roraima, 1000 - 97105-900, Santa Maria, RS, Brazil

<sup>7</sup>Laboratório Interinstitucional de e-Astronomia - LIneA, Rua Gal. José Cristino 77, Rio de Janeiro, RJ - 20921-400, Brazil

<sup>8</sup>Institut Utinam, CNRS UMR 6213, Université de Franche-Comté, OSU THETA Franche-Comté-Bourgogne, Observatoire de Besançon, BP 1615, 25010 Besançon Cedex, France

<sup>9</sup>Department of Astronomy, University of Wisconsin-Madison, Madison, WI 53706, USA

<sup>10</sup>Department of Physics and Astronomy, Bates College, Lewiston, ME 04240, USA

<sup>11</sup>Max-Planck Institute for Astrophysics, Karl-Schwarzschild-Str 1, Garching, Germany 85748

<sup>12</sup>Institute of Cosmology and Gravitation, University of Portsmouth, Dennis Sciama Building, Portsmouth, PO1 3FX, UK

<sup>13</sup>Department of Physics & Astronomy, Johns Hopkins University, Bloomberg Center, 3400 N. Charles St., Baltimore, MD 21218, USA

## ABSTRACT

We present a study of the kinematics of the extraplanar ionized gas around several dozen galaxies observed by the Mapping of Nearby Galaxies at the Apache Point Observatory (MaNGA) survey. We considered a sample of 67 edge-on galaxies out of more than 1400 extragalactic targets observed by MaNGA, in which we found 25 galaxies (or 37%) with regular lagging of the rotation curve at large distances from the galactic midplane. We model the observed  $H\alpha$  emission velocity fields in the galaxies, taking projection effects and a simple model for the dust extinction into the account. We show that the vertical lag of the rotation curve is necessary in the modeling, and estimate the lag amplitude in the galaxies. We find no correlation between the lag and the star formation rate in the galaxies. At the same time, we report a correlation between the lag and the galactic stellar mass, central stellar velocity dispersion, and axial ratio of the light distribution. These correlations suggest a possible higher ratio of infalling-to-local gas in early-type disk galaxies or a connection between lags and the possible presence of hot gaseous halos, which may be more prevalent in more massive galaxies. These results again demonstrate that observations of extraplanar gas can serve as a potential probe for accretion of gas.

*Keywords:* ISM galaxies: kinematics and dynamics galaxies: spiral galaxies

## 1. INTRODUCTION

Warm, ionized gas at high altitude from the midplane has been detected in the Milky Way (Hoyle & Ellis 1963; Reynolds 1971; Reynolds et al. 1973, 1999; Shull et al. 2009). It is also observed in other galaxies (Dettmar 1990; Rand et al. 1990; Rand 1997; Hoopes et al. 1999; Rand 2000; Rossa et al. 2004) at the distances up to several kpc (Rossa & Dettmar 2003; Wu et al. 2014) from galactic midplane. It is one of the tracers indicating significant amounts of extra planar gas. This material is envisioned as an important component of galactic evo-

lution that probes disk-halo interaction (Putman et al. 2012). The material may help support and regulate star formation in galaxies via replenishing gas close to the midplane.

The origin of the extraplanar gas is still unclear. It may have contributions from two sources: cosmological accretion from the intergalactic medium reservoir (Binney 2005), or gas associated with galactic fountain flows in galaxies that are produced by star formation in the disk (Shapiro & Field 1976; Bregman 1980; Norman & Ikeuchi 1989; Marinacci et al. 2011; Fraternali et al. 2013). Both of these effects may be at work together

(Haffner et al. 2009; Benjamin 2012). Since the gas flow motion is either parallel to the sky plane for edge-on galaxies, or obscured by galactic midplane gas, it is difficult to establish from observations if the gas is on the way out or in, caused by fountain flows, or represents some quasi-stable phase of gas energized by continuous activity in the disk. The quantity and distribution of the material suggests the latter, but it does not imply that a connection to flows is not present. Different classes of objects (e.g. AGNs, young stars, old evolved hot stars, or dynamical features) can be responsible for the extra planar gas ionization and motion. Circulation of the gas between the galaxy and the intergalactic medium may be driven by star formation in the disk.

A deviation of the gas component’s rotation from cylindrical at large distances from the midplane, i.e. the rotation velocity lag, or briefly “lag”, has been noticed in several nearby galaxies. It has been measured in the atomic gas (see e.g. Swaters et al. (1997); Matthews & Wood (2003); Zschaechner et al. (2011); Gentile et al. (2013); Kamphuis et al. (2013); Zschaechner & Rand (2015); Zschaechner et al. (2015)), and the ionized gas ((Fraternali et al. 2004; Heald et al. 2006a,b, 2007; Kamphuis et al. 2007, 2011; Rosado et al. 2013; Wu et al. 2014; Boettcher et al. 2016)). The number of galaxies with measured rotation velocity lags is still small, and the lack of data hinders statistical studies. It has been known for a while that a strong correlation exists between star formation per unit disk area and the presence of ionized extra planar gas (Dettmar 2004; Ho et al. 2016), but fewer galaxies have measurements of kinematic lags. An inverse correlation between the lag amplitude and the star formation activity in galaxies was suggested by Heald et al. (2007) but not confirmed by Zschaechner et al. (2011). In this paper we define lag as a decrease in rotational velocity with height.

Studying correlations between the lag and general galactic parameters can be a powerful tool for understanding the nature of the extraplanar gas. The most recent results (Zschaechner & Rand 2015) point at a radially decreasing lag amplitude in galaxies, which the authors interpret as likely pointing at an internal origin of the lags. Lag measurements can also provide potential evidence for accretion of gas onto galactic disks (e.g. Fraternali & Binney (2006, 2008)). Large Integral Field Unit surveys being conducted in recent years (e.g. CALIFA<sup>1</sup>, Sanchez et al. (2016), MaNGA<sup>2</sup>, Bundy et al. (2015), and SAMI<sup>3</sup>, Allen et al. (2015)) provide

excellent data from panoramic spectroscopy suitable for studying the extraplanar gas component in various types of galaxies. In this paper we employ a growing IFU data set from MaNGA survey for studying the kinematics of ionized gas around a substantial sample of edge-on disk galaxies.

## 2. MANGA OBSERVATIONS

MaNGA is a massive integral field unit (IFU) spectroscopic survey (Bundy et al. 2015; Drory et al. 2015) that is part of the fourth phase of the SDSS<sup>4</sup> survey (Blanton et al. 2017). MaNGA plans to deliver  $R \sim 2000$  spectroscopic maps for about ten thousand nearby galaxies by 2020. MaNGA uses the Sloan 2.5 m telescope at Apache Point Observatory (Gunn et al. 2006) and spectrographs that cover the 3600-10300 Å spectral range (Smeed et al. 2013). The survey’s target selection (Law et al. 2015) and observing strategy provide a kiloparsec-scale spatial resolution maps of the stellar and ionized gas kinematics in the galaxies: the resulting FWHM  $\sim 2.5$  arcsec (Law et al. 2016) in the parameter maps corresponds to 1.5 kpc at the median redshift of the survey of 0.03. The observing strategy provides contiguous coverage of targets, without leaving unobserved gaps. The spectra are flux calibrated to the precision of a few percent (Yan et al. 2016). Current data release MaNGA Product Launch - 4 (MPL-4, Westfall et al., in prep., Law et al. (2016)) provides spectral data cubes and various parameter maps derived from them for more than 1400 unique galaxies (including ancillary targets).

### 2.1. *The Sample of Edge-on Galaxies in MaNGA*

Since all MaNGA galaxies were selected based on SDSS imaging products (Law et al. 2015), we were able to download and inspect the color-composite images of all galaxies from SDSS SAS<sup>5</sup> archive (Alam et al. 2015; Blanton et al. 2011). We identified edge-on galaxies from visual inspection similar to how it was done in Bizyaev et al. (2014): objects were classified as edge-on systems if they had no traces of spiral arms that could be seen, and also if the dust lane (if present) was projected on or very close to the galaxy’s disk midplane. We also restricted our search to objects not showing obvious signs of interaction. As a result, we identified 67 edge-on galaxies, without any additional selection by morphological type, size, etc. MaNGA IFUs range in size from 12 arcsec (19-fibers) to 32 arcsec (127-fibers), see the IFU description in Drory et al. (2015). Out of the 67 selected edge-on galaxies, 49% were observed with the largest, 127-fiber

<sup>1</sup> Calar Alto Legacy Integral Field spectroscopy Area survey

<sup>2</sup> Mapping Nearby Galaxies at Apache Point Observatory

<sup>3</sup> Sydney-Anglo-Australian Observatory Multi-object Integral

field survey

<sup>4</sup> Sloan Digital Sky Survey, <http://sdss.org>

<sup>5</sup> Science Archive Server

IFUs, the other 9, 24, 13, and 5% were observed with 91-, 61-, 37-, and 19-fiber IFUs, respectively.

## 2.2. Selecting Edge-on Galaxies with Measurable Rotation Velocity Lag

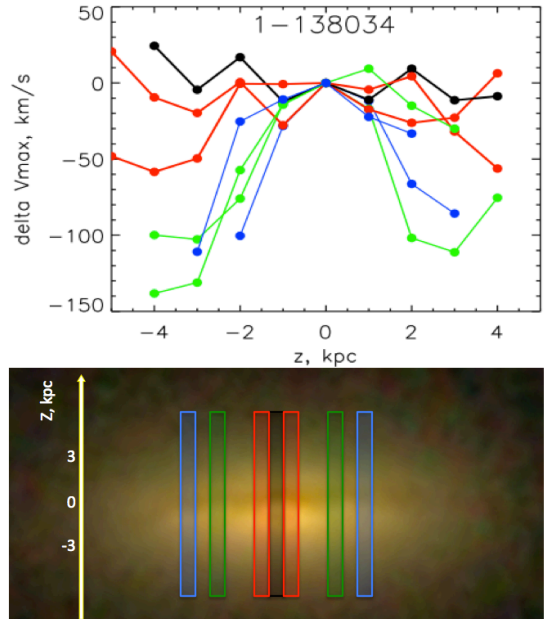
The MPL-4 release provides gas radial velocities estimated for different emission lines on a spatial grid of 0.5 arcsec spaxel size. We utilize  $H\alpha$  fluxes with uncertainties to estimate the signal-to-noise ratio (SNR), and  $H\alpha$  radial velocities with uncertainties for drawing maps of the gas kinematics. In the majority of galaxies the  $H\alpha$  fluxes are detected at higher than 1 kpc altitudes from their galactic midplane. Then we considered the vertical profiles of the radial velocities at different radii from the center, typically in 1-2 kpc wide bins along the major axis. Only the spaxels with good data quality flags and with  $\text{SNR} > 3$  were taken into account. We find that 42 objects in the sample show a rather irregular shape of the vertical velocity profiles, whereas 25 galaxies show a regular decreasing velocity amplitude, i.e. lag, with vertical distance from the midplane, at all radial distances from the center within the limits of our angular resolution of 2.5 arcsec. We refer to this group of galaxies as subsample in the text below, to distinguish it from the main initial sample of edge-on galaxies.

Figure 1 shows two examples of galaxies with vertical velocity profiles that suggest that the rotation curve has lower amplitude above the midplane than in the midplane, i.e. that we observe a lag. The top panel in Figure 1 is a typical galaxy in our sample, while the bottom panel in Figure 1 shows a galaxy with a less clear lag.

We cannot calculate the lag amplitude directly from Figure 1 because of projection effects and possible dust extinction. It is worth noting however, that these effects would not decrease the rotation curve amplitude systematically with altitude above the galactic midplane in the case of pure cylindrical rotation of gas, i.e. in the case of no lag. Thus, we assume that the regular decrease in the gas rotation velocity with vertical distance to the midplane is an indication of a lag. We selected 25 galaxies with regular decreasing velocity amplitude with vertical distance to the midplane for the further modeling.

Images of selected galaxies are shown in Figure 2. It is interesting to note that the IFU size distribution for this subsample well matches that of the overall sample of 67 MaNGA edge-on galaxies: 54, 13, 21, 8, & 4% for 127-, 91-, 61-, 37-, and 19-fiber IFUs, respectively. We will come back to the 42 galaxies that do not show a systematic lag in the discussion in Section 4.

The panels in Figure 2 are 1 arcmin on the side. The largest IFU bundle used for 13 of the 25 galaxies is about half that size. Thus, none of the galaxies are fully covered in the radial extent visible in the figure. This fact implies that we probe the lag mostly over the inner



**Figure 1.** Vertical profiles of radial velocity in two galaxies from our sample. Top panel: the galaxy 1-138034 is shown as a typical example. All velocities are shown with respect to the galactic midplane velocity. The black curve designates the velocity vertical profile that goes through the center ( $X=0$ ). The red curves are for  $X=0.8$  kpc, the green ones correspond to  $X=3$  kpc, and the blue ones designate  $X=4$  kpc. Here  $X$  designates the projected distance to the center along the major axis on the edge-on galaxy. Middle panel: regions used for making the radial velocity profiles in the galaxy 1-138034 designated with the same colors as in the top panel. The background image of the galaxy is taken from SDSS SAS server (see <http://sdss.org>). Bottom panel: same vertical profiles of radial velocity as in the top panel shown for the galaxy 1-282144, in which the lag is seen less clearly.

disk and cannot address with these data if there are radial variations in the lag. At the same time, the data probe well outside the central region and the galactic midplane.



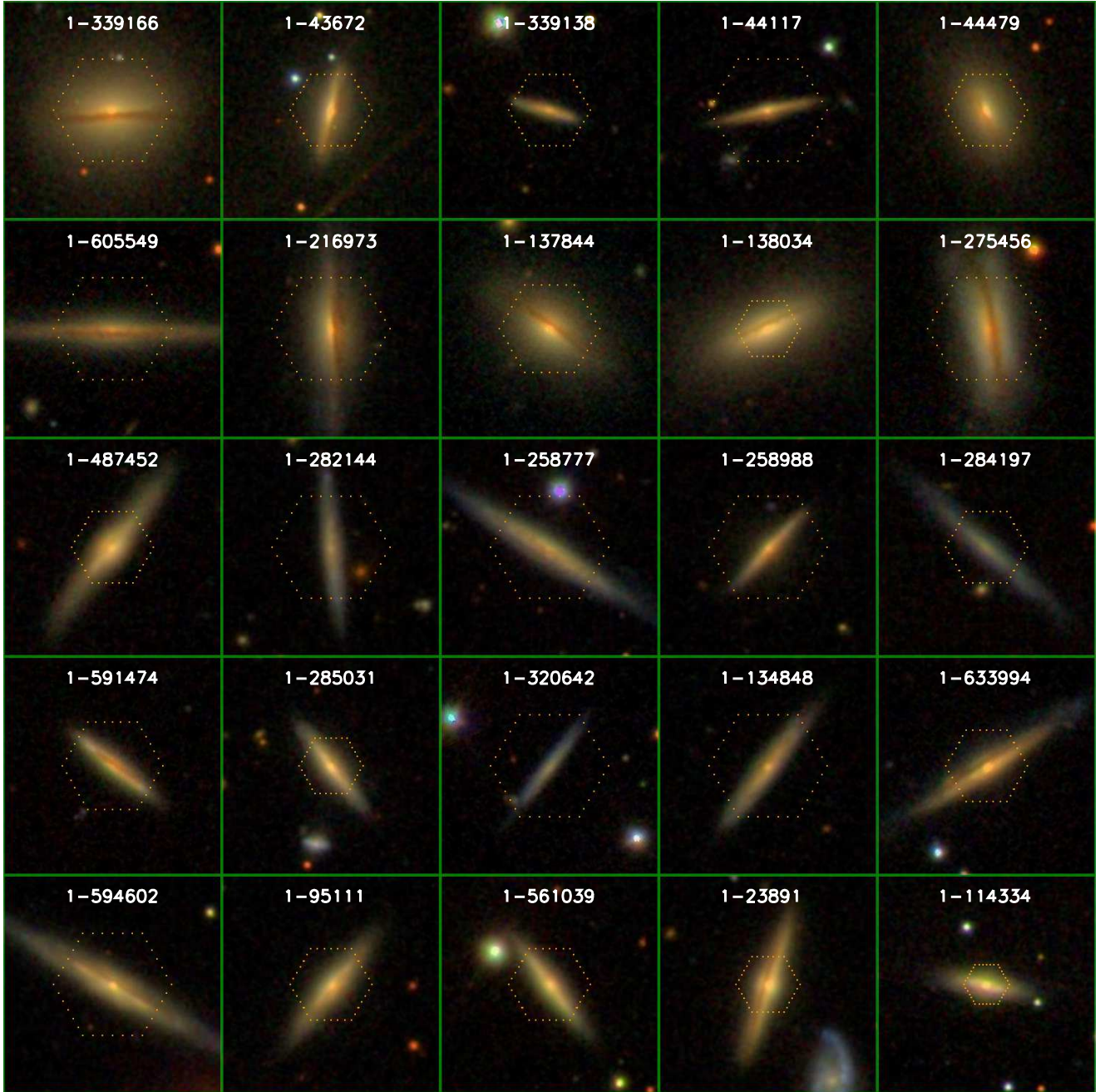


**Figure 2.** Images of selected 25 galaxies with regular lag (see §2.2). The images are taken from the SDSS SAS server (<http://sdss.org>). All objects are shown on the same scale: each individual image has 1 arcmin x 1 arcmin size. The order of the objects is the same as in Table 1: from the top row left to right corresponds to lines 1,2,...5 in Table 1. The 2nd top row in the figure corresponds to lines 6,7,...10 in Table 1, etc. Table 1 is introduced in §3, see below. The yellow dotted contours show the allocation of MaNGA IFUs on the galaxies.

A single fiber corresponds to 1.5 kpc at the median survey redshift. The smallest fiber bundle for this sample (19 fibers) still has 5 fibers across each galaxy. The largest bundle used for more than half the subsample has from 11 to 13 fibers across the major axis of each galaxy, depending on fiber bundle orientation. Coverage decreases away from the center of the galaxy due to the hexagonal shapes of the fiber bundles so the radial extent over which lags may be probed is somewhat smaller than the major axis extent (Drory et al. 2015).

### 3. MODELING IONIZED GAS VELOCITY FIELDS

Below we assume that the ionized gas that emits  $H\alpha$  follows a bi-exponential 3-dimensional distribution in the galaxy, and introduce its rotation curve as an analytical function. We construct model maps of the two-dimensional distribution of  $H\alpha$  radial velocities by integrating the volume density weighted  $H\alpha$  emission profiles along the line of sight. Then we compare the resulting  $H\alpha$  velocity fields with observations and obtain the model parameters via chi-square optimization.

The model rotation curve in the midplane is approximated by three parameters: radius  $r_0$  to which the velocity rises linearly, the rotation velocity at  $r_0$ ,  $V_{max}$ , and the gradient of the rotation curve beyond the  $r_0$ ,  $dv/dr$ . The latter allows for the possibility of a slightly rising or decreasing rotation curve. Hence,  $V(r) = V_{max} \cdot (r/r_0)$ , if  $r < r_0$ , and  $V(r) = V_{max} + dv/dr \cdot (r - r_0)$ , if  $r \geq r_0$ , where  $r$  is the distance to the galactic center.

The lag of the rotation velocity is introduced as a linear vertical gradient  $dv/dz$ :  $V(r, z) = V(r) - |z| \cdot dv/dz$ , where  $z$  is the vertical distance in kpc. The rotation curve and the lag are assumed independent of the polar angle in the disk plane,  $\phi$ . Since the observed rotation curve is a result of projection of  $V(r, \phi, z)$  on the sky plane, we have to consider the line-of-sight integration of  $V(l, z)$  weighted by the  $H\alpha$  luminosity volume density  $f_{H\alpha}$ . Here  $l(r, \phi)$  designates the distance along a particular line of sight.

We assume that the distribution of the  $H\alpha$  luminosity density is a double exponential:  $f_{H\alpha}(r, z) = f_0 \exp(-r/h) \exp(-|z|/z_0)$ , where the scale length  $h$ , scale height  $z_0$ , and  $f_0$  are estimated from the  $H\alpha$  maps of the galaxies using the structural parameters pipeline used in Bizyaev & Mitronova (2002, 2009); Bizyaev et al. (2014). The  $H\alpha$  maps are obtained from the fluxes provided by MPL-4.

We also introduce a dust disk embedded in the galactic disk (co-planar with the ionized gas and stellar disks). The dust extinction coefficient  $\kappa(r, z) = \kappa_0 \exp(-r/h_d) \exp(-|z|/z_d)$  is the volume extinction coefficient at the  $H\alpha$  wavelength in a certain point  $(r, z)$  in the disk,  $h_d$  and  $z_d$  are the radial and vertical disk scales, and  $\kappa_0$  is the value of the extinction coefficient in the

center. We neglect dust scattering in the sense that we treat  $\kappa$  as a volume absorption coefficient and ignore the possibility that scattered light might contribute along a line of sight.

We assume that each point  $(r, \phi, z)$  in the model disk produces an emission line profile with the central wavelength that corresponds to its velocity  $V(r, z)$  and the peak height proportional to the luminosity volume density. We assume the same velocity dispersion  $\sigma_w = 10 \text{ km s}^{-1}$  for all local Gaussian profiles at each  $(r, \phi, z)$ . For the radial velocity profile in each point in the disk  $v_p(w, r, \phi, z)$ , we assume that  $v_p(w, r, \phi, z) = V(r, z) \exp(-w^2/2\sigma_w)$ . Here  $w$  is the offset of the radial velocity from the peak velocity  $V(r, z)$ , and  $w=0$  at the peak. If  $X$  and  $Y$  are the radial (along the major axis) and vertical (along the minor one) coordinates in the sky plane, the integrated velocity profile  $V_p$  can be written

$$V_p(w, X, Y) = \int_{-L}^L v_p(w, r(l), z) \cos(\phi(l)) f_{H\alpha}(r(l), z) e^{-\tau(r(l), z)} dl, \quad (1)$$

where

$$\tau(r(l), z) = \int_l^L \kappa(r(l), z) dl, \quad (2)$$

and  $\cos(\phi(l))$  accounts for the projection of the velocity vector on the line of sight, and the integration along the line of sight is towards our position starting from the far side of the disk. The vertical axis  $z$  is aligned with the sky plane axis  $Y$ , so  $Y = z$ . The limits of integration in  $L$  correspond to  $r = 4h$ , by analogy with stellar disks that truncate at their four radial scales, on average.

After the integration along the line of sight we obtain a resulting emission line profile  $V_p(w)$  of the radial velocity spaced at a set of spaxels  $(X, Y)$ . The emission line profile is convolved with a Gaussian kernel with FWHM of the spectral resolution. To obtain the final "observable" distribution of the radial velocities in the sky plane, we convolve the  $V(X, Y)$  with a two-dimensional Gaussian point spread function (PSF) whose FWHM corresponds to the effective FWHM estimated by the data reduction pipeline for each data cube (Law et al. 2016). Then we estimate the corresponding radial velocity  $V(X, Y)$  by fitting the radial velocity profile around the peak velocity value with a Gaussian function.

We estimate the free model parameters via chi-square minimization using the downhill simplex "amoeba" optimization algorithm (Nelder & Mead 1965). The observing uncertainty of the radial velocity was corrected for the minimum gas velocity dispersion by adding the expected gas velocity r.m.s.,  $10/\sqrt{3} \text{ km s}^{-1}$  in quadra-

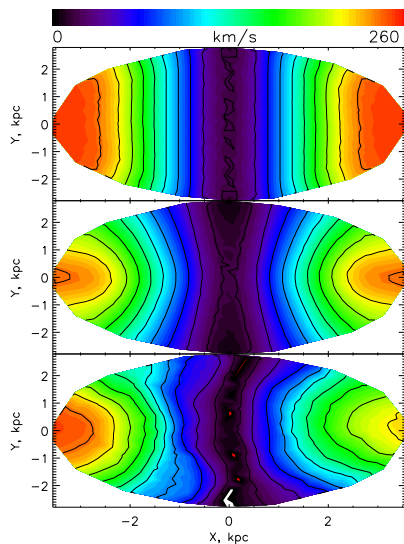


**Figure 3.** Absolute values of velocity fields of our typical galaxy 1-138034: model field in the case of fitting with no vertical lag (top), model field with lag (middle), and the observed velocity field (bottom).

ture. We also applied spaxel quality flags provided by the pipeline: only spaxels with good data reduction flags and with  $\text{SNR} > 3$  were included into the minimization. The free parameters of the model are  $V_{max}$ ,  $r_0$ ,  $dv/dr$ ,  $dv/dz$ ,  $\kappa_0$ , and also the central radial velocity  $V_0$ . We don't expect any degeneration between the parameters, so we did not apply any observational constraints to them except a natural requirement of the positivity of  $V_{max}$ ,  $r_0$ , and  $\kappa_0$ . We fixed the dust disk structural parameters as  $z_d = z_0$  and  $h_d = h$ , which is equivalent to the assumption of uniform mixing of the ionized gas and dust. For comparison, we ran the same modeling for the cases of uniformly distributed ionized gas volume density along the  $r$  and  $z$ . Also we considered shorter vertical and longer radial scales of the dust  $z_d = 0.5 z_0$  and  $h_d = 1.5 h$ , and also  $h_d = 2 h$  and  $h_d = h$  (following Xilouris et al. 1999; Kylafis et al. 2001; Matthews et al. 1999; Yoachim & Dalcanton 2006; Bianchi 2007). In all cases considered the resulting model parameters were within 15% of the original model, which suggests low sensitivity of the output to the input assumptions on the distribution of ionized gas and dust. The lag values derived from the model fits are shown in Table 1.

Figure 3 shows the best-fit model velocity field for the same galaxy shown in Figure 1 for the case of models with no lag and with lag (top and middle panels respectively). The model simultaneously fits lags in the "left" and "right" parts of the galaxy (with respect to the minor axis), so the absolute values of the radial velocity are shown for clarity of presentation. The observed velocity

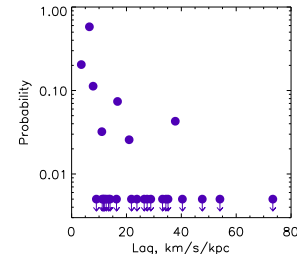


**Figure 4.** Probabilities of the null hypothesis that models with and without a rotation velocity lag would statistically result in the same chi-square values (i.e. that chi-square does not decrease enough to justify the additional parameter to model a lag). A few models with small lags show a high probability for no difference, while the bulk of the models gain from using the lag as an additional free parameter. The smallest values of the probabilities are shown as upper limits at 0.5% for clarity in the figure.

field strongly favors the case with the vertical rotation curve lag.

### 3.1. Robustness of the Modeling

To estimate the robustness of our results, we ran the same models with zero, fixed lag term,  $dv/dz=0$ . Then we performed F-tests using the same sample of galaxies modeled with and without lags. Figure 4 shows the probability that chi-square values are significantly similar between the lag and no-lag models. Note that most of the probability values are very low, so we truncated the values in Figure 4 at 0.5% for better presentation. As expected, for several galaxies in the subsample with small lags ( $10 \text{ km s}^{-1} \text{ kpc}^{-1}$  and less) the chi-square do not change significantly, whereas models of the galaxies with large lags fit much better when a rotation velocity vertical gradient is introduced.

We also constructed a set of synthetic galaxies with typical parameters  $h$ ,  $z_0$ ,  $h_d$ ,  $z_d$ ,  $\kappa_0$ ,  $V_{max}$ ,  $dv/dr$ , and  $dv/dz$ . For each case the distribution of radial velocity projected on the sky plane and convolved with observed the PSF was derived. We added normally distributed uncertainties to the radial velocities in each spaxel. We also added typical noise to the fluxes in each spaxel. For the latter we used the MaNGA observations completion criterion from the science requirement document (Bundy et al. 2015; Law et al. 2015), which states that  $\text{SNR}=5$  has to be obtained at  $1.5 R_e$  (effective radii) for all program galaxies. We considered a set of noise levels scaled by  $\text{SNR} = 1, 2, 3, 5, \text{ and } 10$  at  $1.5 R_e$ . For each



set of galactic parameters and noise levels, we made 30 synthetic galaxies and estimated their parameters with the pipeline described above.

We obtain that the lag gradient  $dv/dz$  is one of the most reliable parameters estimated by the minimization. Its typical uncertainty is 10-15%. When we convert this uncertainty to the actual lag in velocity  $dV/dz = dv/dz \cdot V_{max}$ , the rotation curve amplitude uncertainty increases the uncertainty on the lag to 20%. The other reasonably estimated model parameters are the radial velocity gradient  $dv/dr$  and  $V_{max}$ . The value  $r_0$  has uncertainty of 15%, but in some cases it is shifted systematically against the true initial value in different directions for different model parameters, which increases the uncertainty of this parameter up to 25%. The least reliable parameter is the dust absorption coefficient  $\kappa_0$ , which is often underestimated in the modeling, and its uncertainty sometimes reaches 100%. Nevertheless, it does not affect the inferred rotation curve lag because the high altitude regions in the galaxies, which are good tracers of the lag, are less affected by the dust extinction. Figure 5 shows a result of the modeling for a typical set of the model parameters. We conclude that the uncertainty of our rotation velocity lag estimation is 20%. We are also inclined to add a low threshold of  $6 \text{ km s}^{-1} \text{ kpc}^{-1}$  to this uncertainty based on Figure 4, which suggests that given the uncertainty and resolution of the data, the modeling procedure does not seem sensitive to variations of the lag below  $6 \text{ km s}^{-1} \text{ kpc}^{-1}$ .

### 3.2. Inclination Effects

Since our modeling assumes  $90^\circ$  inclination of galactic disks to the line of sight, any deviation from the perfect edge-on inclination may affect parameters estimated in any studies of edge-on galaxies. [deGrijs et al. \(1997\)](#) showed that the photometric vertical scale height increases by 20% if the inclination  $i$  deviates from the  $90^\circ$  by  $5^\circ$ . We use the visibility of the dust lane in SDSS images of all selected galaxies with lags and simple technique described in [Bizyaev & Kajsin \(2004\)](#); [Mosenkov et al. \(2015\)](#) to estimate the inclination. We do not see any dependence between the lag and the inclination. We find that only three galaxies have  $i < 85^\circ$ : 1-561039, 1-339138, and 1-114334. The latter has  $i \approx 82^\circ$ , and we excluded it from the further analysis. The galaxies 1-561039 and 1-339138 have  $i$  between 84 and  $85^\circ$ . Although they do not change trends in figures with the lag shown below in this paper, we excluded them from the figures.

In order to estimate how large the projection due to non-edge-on orientation is in the galaxies, we compare the "projection size" in the galaxies (explained below in this paragraph) with the spatial resolution of MaNGA data cubes. The latter is assumed to be  $\text{FWHM}/2.35$ ,

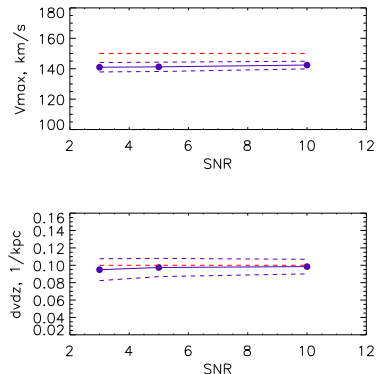


**Figure 5.** The input (red dashed line) and the output model parameters (blue curves) estimated for the set of synthetic galactic images after inserting noise in them, see text. The solid curves with bullets designate the mean parameters, and the dashed blue curves show 1-sigma standard deviation of the parameters in the set of the models with the same SNR. The ranges of the vertical axes correspond to the typical values of the parameters in our modeling.

which corresponds to the spatial "sigma" resolution in the MaNGA images, see §2). The "projection size" is calculated as the diameter of galactic disk in projection on the sky plane due to the inclination. We find that the overlap between the near and far sides of galactic disks is less than the spatial resolution in our data for all objects. Thus we conclude that the inclination effects can be ignored for our subsample. In general, the inclination affects are important and have to be considered when subsamples of edge-on galaxies are formed from the future MaNGA sample.

## 4. RESULTS AND DISCUSSION

We started with a sample of 67 galaxies and found that 25 show systematic patterns in the velocity field suggesting a lag is present. Note that we are not claiming that the other 42 galaxies do not show any lag, only that upon inspection of the velocities it appears less regular and therefore less suitable to the modeling approach we have adopted in this paper.

Previous work in measuring lags for ionized or neutral atomic gas have involved smaller samples of galaxies. Ours is the first study of a moderately large sample of observed with one particular IFU setup and analyzed the same way. The large sample offers opportunities for investigating trends in lags with integral galactic parameters described below.



The lags are expected as result of galactic fountain flows, but ballistic models of such flows indicate much smaller lags than observed (Collins et al. 2002; Fraternali & Binney 2006). An inverse correlation between the lag amplitude of ionized gas and the star formation activity in galaxies was suggested by Heald et al. (2007). The inverse correlation was not seen in the neutral gas phase (see Zschaechner & Rand 2015, and references therein). Surprisingly, no clear trends have been found between lag and other galaxy properties so far. In particular, lags have not been seen to correlate with star formation rate, strength of gravity, or environment. The most recent results (Zschaechner & Rand 2015; Zschaechner et al. 2015) point at a radially decreasing lag amplitude in the neutral gas in galaxies, which the authors interpret as likely pointing at an internal origin for the lags. Our radial coverage is limited so we cannot yet address radial variations, but here we consider correlations with star formation rates and global galaxy properties for our subsample of galaxies with lag.

To characterize the star formation rate and star formation rate surface density, we considered the integrated WISE band 4 ( $22\ \mu\text{m}$ ) luminosities for the two subsamples. This WISE band has been shown to accurately track the SFR (e.g. Relano et al. 2007; Zhu et al. 2008; Jarrett et al. 2013) in HII regions and galaxies. The  $H\alpha$  luminosities would underestimate the total SFR due to extinction and lack of coverage of the outer disk in the IFU spectra. We discuss both effects below for the subsample of 25. The two subsamples showed similar distributions both in total SFR and SFR/area.

We also considered the distribution of axial ratios ( $b/a$ ) provided in the NSA for the galaxies (here we use the axis ratio  $b/a$  from Stokes parameters at 50% light radius). Interestingly, all galaxies while clearly edge-on or close to edge-on, show a full range in  $b/a$  from 0.3 to 0.9. There is a difference in the histogram of  $b/a$ : the subsample of 42 shows a peak around  $b/a$  of 0.4, which is not seen in the subsample of 25. This difference suggests that the fraction of galaxies with less prominent bulge/spheroidal components is larger in the sample of 42 galaxies without regular lags.

We will now analyze trends for the subsample of galaxies where we derived a robust lag value. Figure 6 shows the relationship between the total  $H\alpha$  luminosity and the lag. The luminosity is estimated by the integration of the total  $H\alpha$  flux in the galaxies from MaNGA data. As mentioned above, this estimate may be incomplete due to IFU coverage and it will certainly suffer from extinction. We see no clear correlation (with negative correlation coefficient  $cc = -0.17$ ). The lack of correlation was also apparent when we replaced the  $H\alpha$  luminosity with the mean surface density of the the  $H\alpha$  luminosity ( $H\alpha$  luminosity divided by the disk area, where the disk

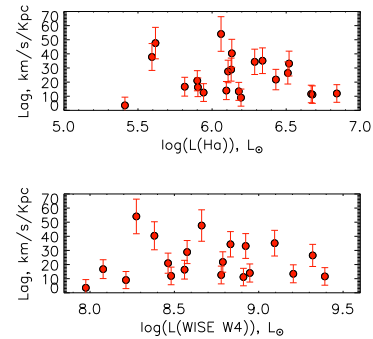


**Figure 6.** Top: the total  $H\alpha$  luminosity in the galaxies and the rotation curve lag. The luminosity is not corrected for the internal extinction. Bottom: Lag versus the luminosity of the galaxies in the WISE W4 band. The W4 luminosity should correlate well with the star formation rate in the galaxies.

area was derived using the scale length of the  $H\alpha$  disk; figure not included).

A better indicator of global star formation in the case of edge-on galaxies is the infrared (IR) luminosity and in particular the band 4 WISE luminosity, as discussed above. We calculated the IR luminosity in the WISE W4 band (at  $22\mu$ ), which is very likely optically thin. The WISE fluxes for the galaxies are taken from the ALLWISE catalog (Wright et al. 2010). We find that the  $H\alpha$  and W4 luminosities are linearly correlated, although with significant scatter. The average ratio between W4/ $H\alpha$  luminosities for this subsample is about ten times larger than what is seen in face-on galaxies, consistent with larger extinction of the  $H\alpha$  emission in edge-on systems and with incomplete  $H\alpha$  coverage.

The bottom panel in Figure 6 indicates that there is no correlation ( $cc = -0.04$ ) between the rotation velocity lag and the star formation rate traced by the IR luminosity, a result similar to the  $H\alpha$  data. The lack of the clear correlation between the star formation rate and the lag amplitude is not necessary an indicator that there must be an external source of ionization of the gas at high altitudes. We observe a correlation ( $cc = 0.55$ ) between the vertical scale heights of the ionized gas and the star formation rates, as probed by the total  $H\alpha$  luminosity, see Figure 7. This correlation suggests that internal galactic sources likely play a large role in ionizing gas at high altitudes consistent with previous studies.

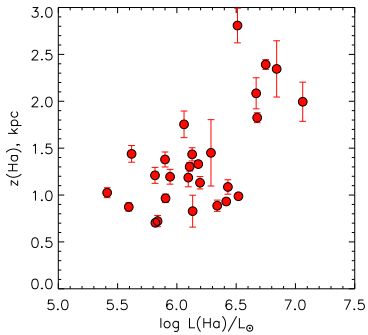


**Figure 7.** The vertical scale height of the ionized gas versus the total  $H\alpha$  luminosity in the galaxies.

Figure 8 demonstrates a noticeable correlation between the lag and the stellar mass of galaxies ( $cc = 0.50$ ). The mass in the upper panel is the stellar mass estimated in the NASA-Sloan Atlas of galaxies (NSA<sup>6</sup>). The lower panel in Figure 8 shows the central stellar velocity dispersion from the NSA ( $cc = 0.55$ ). Both values are estimated for NSA from earlier SDSS data, independent of MaNGA. The stellar mass is expected to correlate strongly with the total dark matter halo mass (e.g. Behroozi et al. (2013)). We also observe significant correlation between the lag and the maximum rotation velocity in the galaxies  $V_{max}$  ( $cc = 0.55$ , not shown here). The latter is expected: large amplitude lags are easier to detect in galaxies with circular velocities much larger than the total lag.

We considered several additional global parameters of the galaxies in the analysis. A correlation between the lag value and the axial ratio of the star light for the galaxies (estimated in NSA) can be seen in Figure 9 ( $cc = 0.48$ ). Less significant is correlation with the NSA Sersic index of the galaxies ( $cc = 0.26$ ). Both parameters are relevant to morphological type of galaxies, and suggest that we tend to observe the largest lag values in early-type disk galaxies.

Active Galactic Nuclei (AGN) could affect our results by contributing to the  $H\alpha$  luminosity via adding a non-star formation-relevant component, as well as to the motion and ionization status of extraplanar gas in the cen-

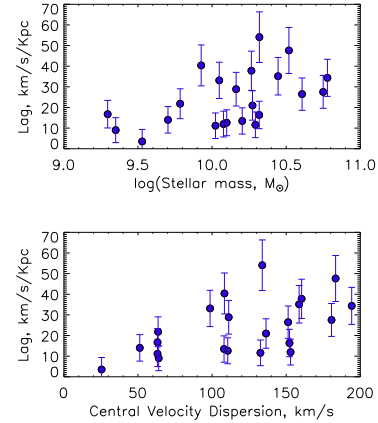


**Figure 8.** Top panel: the rotation curve lag versus the stellar mass estimated in the NSA atlas. Bottom panel: the rotation curve lag versus the central velocity dispersion in the galaxies .

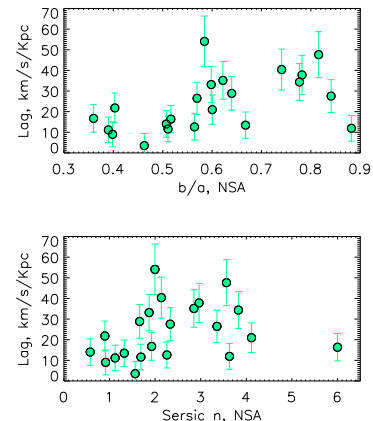


**Figure 9.** Top panel: the rotation curve lag versus the flatness of the galaxy, as estimated by the NSA atlas. Bottom panel: the rotation curve lag versus the galactic Sersic index from the NSA atlas.

tral regions. The former factor can be neglected: we excluded the central 3 arcsec diameter regions from the calculation of the  $H\alpha$  luminosity and observed the same trends as in Figure 8, which is not surprising since the mean ratio of the excluded luminosity to the total is only 0.04 in our galaxies and an AGN would likely not

<sup>6</sup> <http://nsatlas.org>

be directly seen in an edge-on system.

Most of our galaxies from both subsamples (with and without regular lags) were classified with "BPT types" (named after Baldwin, Phillips, and Terlevich, [Baldwin et al. 1981](#)) in the MPA-JHU catalog<sup>7</sup> (see e.g. [Brinchmann et al. 2004](#)). Note that the classification was made with SDSS spectra, which were obtained from the 3-arcsec central region in galaxies. The BPT types are: 1- star-forming, 2 - low signal-to-noise star-forming, 3 - composite, 4 - AGN (excluding liners), and 5 is a LINER. To summarize them, 1-2 describes the central star forming dominated galaxies, while 4-5 designate the presence of a nuclear activity. [Figure 10](#) demonstrates the distribution of the galaxies with regular lags and those without regular lag by BPT type. We see that both galaxy subsamples contain all BPT types, but the galaxies that do not show a regular lag have a larger fraction of galaxies dominated by star formation. While this difference seems suggestive of a role for an AGN, we note that BPT types for edge-on systems are likely inaccurate due to extinction. The trend here is likely more consistent with the earlier noted difference in axial ratios for the two subsamples: the non-regular lag subsample includes more pure disk galaxies which are less likely to have AGN or LINER type emission in their central region. It may also be simply related to the trend with stellar mass: more massive galaxies are more likely to have an AGN. While the composite and AGN/LINER galaxies all show regular lags, the star formation-dominated galaxies show mostly no regular lags.

Lastly, we considered the distribution of derived lags with the range in radius over which the fits were executed. We looked at both the linear range in kpc and the scaled range in radius normalized by derived radial scale length. For the 25 galaxies, the range in radius over which the fits were done is between 3 to 20 kpc. This large range takes place due to various factors: the spread in distance for the galaxies, their intrinsic disk sizes, and the size of the IFU bundles. This variety makes it difficult to interpret trends. The one factor that stood out is that the largest lags (over  $30 \text{ km s}^{-1} \text{ kpc}^{-1}$ ) were found only for galaxies for which the total fitting radius was less than 10 kpc. It is possible that this trend is consistent with the general decrease found in vertical lags with distance from the center for the HI distribution across single galaxies ([Zschaechner & Rand 2015](#)). That is, for galaxies that are large enough and well enough covered by the IFU such that the radial range of our fits extends out to between 10 and 20 kpc on average, we find lower

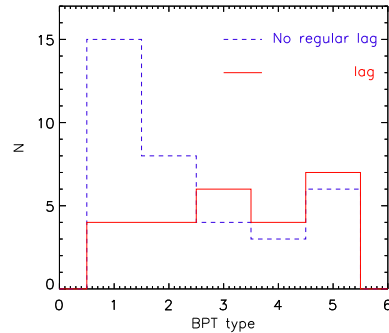


**Figure 10.** The BPT types determined from spectra of the central regions in galaxies by the MPA-JHU catalog (see text). The blue dashed curve shows the distribution of galaxies without regular rotation lags, while the red solid red line that for for the galaxies with regular lags in the extra planar ionized gas. The BPT types 1-2 indicate the star forming galaxies, while types 4-5 designate AGN/LINER classes (see text for detail).

overall lag values than for galaxies where the fit range is smaller than 10 kpc in radius. The trend, however, is not seen when the radial range of the fit is expressed in radius normalized with the disk scalelength. We will need a larger sample and more deeply consider coverage of the IFU versus total disk extent of the galaxies to probe such trends further.

The lag amplitude does not correlate strongly with the BPT type as we show in [Figure 11](#), although it can be noticed that the largest lags in our subsample are observed in the galaxies with high BPT classification, hence potential AGN activity, while small lags (under  $20 \text{ km s}^{-1} \text{ kpc}^{-1}$ ) occur equally often in star-forming and in mild AGN/LINER galaxies.

## 5. SUMMARY AND CONCLUSIONS

To summarize, we observe a correlation of the lag amplitude with the stellar mass (and therefore likely also with halo mass), with the central velocity dispersion, and also with galaxy type traced by the stellar disk flatness and global Sersic index. We see no correlation between the lag and the star formation activity in galaxies in the plots of the lag versus the  $H\alpha$  and IR luminosity in [Figure 6](#). According to [Figure 9](#), late type disk galaxies tend to have smaller lags, and more often than the early-type disk systems they show no regular lags. It is plausible that larger lags in early type disk

<sup>7</sup> a collaborative project that involved Max-Planck Institute for Astronomy and Johns Hopkins University

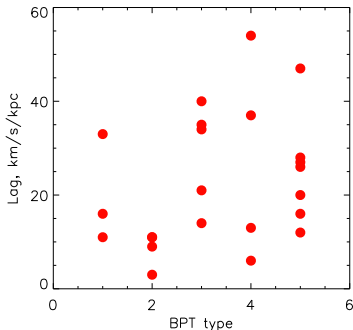


**Figure 11.** The rotation lag versus the BPT type. The latter was determined by the MPA-JHU catalog in the central 3-arcsec region.

galaxies with higher mass may be related to the higher infalling-to-local gas ratio in these systems compared to lower mass galaxies. Such accreting gas may come from the intergalactic medium or, alternatively, such massive galaxies are more likely to have prominent intrinsic hot gaseous halos that may interact with the disk-halo gas to produce lagging velocities. [Marinacci et al. \(2011\)](#) modeled the effect of such a hot halo on the extraplanar gas kinematics. They found that interaction at the interface between clouds and the hot halo may lead to cooling of gas from the hot gas reservoir and subsequent infall into disks. [Fraternali et al. \(2013\)](#) showed that supernova driven galactic fountains can transport gas from hot halo down to the galactic disk. Whether the accretion is from a pre-existing hot gaseous halo or directly from the IGM, the lags we observe may provide indirect evidence for accretion of gas. Since the external gas would have slower rotation with respect to the gas in galactic disks, accretion of significant amounts of the gas will create noticeable lags, i.e. the higher the ratio of infalling-to-local gas, the larger the lag we observe. Although this explanation is plausible, additional observations and simulations are necessary to confirm.

We performed modeling of the ionized gas radial velocities and emission line fluxes provided by MaNGA data analysis pipeline MPL-4. Our models were designed to derive the vertical lag of the ionized gas rotation velocity that is observed in velocity fields of the gas.

We selected a sample of 67 edge-on galaxies from more than 1400 galaxies observed by MaNGA. In 25 galaxies of this sample (i.e. in 37%) we observe a regular lag of

the rotation curve in the extraplanar gas. We derived the lag in the 25 galaxies that span a wide range of masses and luminosities.

We observe no correlation between the amplitude of the lag and galactic star formation activity traced by  $H\alpha$  and IR luminosity. At the same time, the lag demonstrates a noticeable correlation with galactic stellar mass, hence dark matter halo mass, and central stellar velocity dispersion. The lags are larger in early-type disk galaxies, whereas smaller lag values are more typical for late-type galaxies. Early-type galaxies are known to be gas-poor, while late-type galaxies contain more gas. We interpret our results as evidence for a higher ratio of infalling-to-local gas in early-type galaxies and, in general, the data may point at the importance of gas infall in the galactic gas balance.

As the MaNGA observing campaign proceeds, we expect to increase our sample of the galaxies with measured lags by a factor of five (given MaNGA observing goals), and to build the largest ever sample of galaxies available for statistical studies of the rotation velocity lags in the extraplanar ionized gas. Accretion from an IGM might not lead to symmetric velocity lags, whereas interaction with hot halo gas might. Our future studies will therefore also in more detail address the properties of the galaxies that do not show regular lag and study the possible difference in the lags above and below disks to distinguish between the different scenarios.

This material is based on work partially supported by the National Science Foundation under Grant No. AST-1615594 to RAMW. AD acknowledges support from The Grainger Foundation. DB acknowledges support from RSF grant RSCF-14-50-00043. We appreciate anonymous referee for valuable suggestions that improved the paper.

SDSS- IV acknowledges support and resources from the Center for High-Performance Computing at the University of Utah. The SDSS web site is [www.sdss.org](http://www.sdss.org).

SDSS-IV is managed by the Astrophysical Research Consortium for the Participating Institutions of the SDSS Collaboration including the Brazilian Participation Group, the Carnegie Institution for Science, Carnegie Mellon University, the Chilean Participation Group, the French Participation Group, Harvard-Smithsonian Center for Astrophysics, Instituto de Astrofísica de Canarias, The Johns Hopkins University, Kavli Institute for the Physics and Mathematics of the Universe (IPMU) / University of Tokyo, Lawrence Berkeley National Laboratory, Leibniz Institut für Astrophysik Potsdam (AIP), Max-Planck-Institut für Astronomie (MPIA Heidelberg), Max-Planck-Institut für Astrophysik (MPA Garching), Max-Planck-Institut für



Extraterrestrische Physik (MPE), National Astronomical Observatory of China, New Mexico State University, New York University, University of Notre Dame, Observatorio Nacional / MCTI, The Ohio State University, Pennsylvania State University, Shanghai Astronomical Observatory, United Kingdom Participation Group,

Universidad Nacional Autónoma de México, University of Arizona, University of Colorado Boulder, University of Oxford, University of Portsmouth, University of Utah, University of Virginia, University of Washington, University of Wisconsin, Vanderbilt University, and Yale University.

## REFERENCES

- Alam, Sh., Albareti, F. D., Allende Prieto, C. et al. 2015, *ApJS*, 219, 12
- Allen, J. T., Croom, S. M., Konstantopoulos, I. S. et al. 2015, *MNRAS*, 446, 1567
- Baldwin, J. A., Phillips, M. M., & Terlevich, R., 1981, *PASP*, 93,5
- Behroozi, P. S., Wechsler, R. H., & Conroy, C. 2013, *ApJ*, 770, 57
- Benjamin, R. A., 2012, *EAS Pub. Ser.*, 56, 299
- Bianchi, S. 2007, *A&A*, 471, 765
- Binney, J. 2005, in *Extra-planar Gas Conference*, ed. R. Braun, *ASP Conf. Ser.*, 331, 131
- Bizyaev, D. & Kajsin, S. 2004, *ApJ*, 613, 886
- Bizyaev, D. & Mitronova, S. 2002, *A&A*, 389, 795
- Bizyaev, D. & Mitronova, S. 2009, *ApJ*, 702, 1567
- Bizyaev, D., Kautsch, S., Mosenkov, et al. 2014, *ApJ*, 787, 24
- Blanton, M. R., Kazin, E., Muna, D. et al. 2011, *AJ*, 142, 31
- Blanton, Michael R., Bershady, Matthew A., Abolfathi, Bela, Albareti, Franco D. et al. 2017, *arXiv:1703.00052*
- Boettcher, E., Zweibel, E., Gallagher, J. S. III, & Benjamin, R., *arXiv:1609.07491*
- Bregman, J. N. 1980, *ApJ*, 236, 577
- Brinchmann, J., Charlot, S., White, S. D. M., Tremonti, C. et al. 2004, *MNRAS*, 351, 1151
- Bundy, Kevin; Bershady, Matthew A.; Law, David R.; 2015 *ApJ*, 798, 7
- Collins, J. A., Benjamin, R. A., & Rand, R. J. 2002, *ApJ*, 578, 98
- de Grijs, R., Peletier, R. F., & van der Kruit, P. C., 1997, *A&A*, 327, 966
- Dettmar, R.-J., 1990, *A&A*, 232, L15
- Dettmar, R.-J., 2004, *Astrophysics and Space Science*, 289, 349
- Drory, N.; MacDonald, N.; Bershady, M. A.; Bundy, 2015 *AJ*, 149, 77
- Fraternali, F., Oosterloo, T., & Sancisi, R. 2004, *A&A*, 424, 485
- Fraternali, F., & Binney, J. J., 2006, *MNRAS*, 366, 449
- Fraternali, F., & Binney, J. J., 2008, *MNRAS*, 386, 935
- Fraternali, F., Marasco, A., Marinacci, F., & Binney, J., 2013, *ApJ*, 764, 21
- Gentile, G., Jzsa, G. I. G., Serra, P., et al. 2013, *A&A*, 554, 125
- Gunn, J. E., Siegmund, W. A., Mannery, E. J. et al. 2006, *AJ*, 131, 2332
- Haffner, L. M., Dettmar, R.-J., Beckman, J. E., Wood, K., et al. 2009, *Rev. Mod. Phys.*, 81, 969
- Heald, G. H., Rand, R. J., Benjamin, R. A., et al. 2006, *ApJ*, 636, 181
- Heald, G. H., Rand, R.J., Benjamin, R. A., Bershady, M. A., 2006, *ApJ*, 647, 1018
- Heald, G. H., Rand, R. J., Benjamin, R. A., Bershady, M. A., 2007, *ApJ*, 663, 933
- Ho, I.-T., Medling, A. M., Bland-Hawthorn, J., Groves, B. et al. 2016, *MNRAS*, 457, 1257
- Hoopes, C. G., Waltherbos, R. A. M., Rand, R. J., 1999, *ApJ*, 522, 669
- Hoyle, F. & Ellis, G. R. A. 1963, *Aust. J. Physics*, 16, 1
- Jarrett, T. H., Masci, F., Tsai, C. W., et al., 2013, *AJ*, 145, 6
- Kylafis, N., Misiornis, A., Papamastorakis, J., & Xilouris, E. 2001, *Astrophysics and Space Sci.*, 276, 531
- Kamphuis, P., Peletier, R. F., Dettmar, R.-J., et al. 2007, *A&A*, 468, 951
- Kamphuis, P., Peletier, R. F., van der Kruit, P. C., & Heald, G. H. 2011, *MNRAS*, 414, 3444
- Kamphuis, P., Rand, R. J., & Jzsa, G. I. G. 2013, *MNRAS*, 434, 2069
- Law, David R.; Yan, Renbin; Bershady, Matthew A. et al. *AJ*, 150, 19
- Law, D. R., Cherinka, B., Yan, R., Andrews, B. H. et al. 2016, *AJ*, 152, 83
- Marinacci, F., Fraternali, F., Nipoti, C. et al. 2011, *MNRAS*, 415, 1534
- Matthews, L. D., Gallagher, J. S., & van Driel, W. 1999, *AJ*, 118, 2751
- Matthews, L. D. & Wood, K. 2003, *AJ*, 593, 721
- Mosenkov, A. V., Sotnikova, N. Ya., Reshetnikov, V. P., Bizyaev, D. et al. 2015, *MNRAS*, 451, 2376
- Nelder, J.A. & Mead, R. 1965, *Computer Journal*, 7, 308
- Norman, C. A. & Ikeuchi, S. 1989, *ApJ*, 345, 372
- Putman, M. E., Peek, J.E.G., & Joung, M.R. 2012, *ARA&A*, 50, 491
- Rand, R. J., Kulkarni, S. R., & Hester, J. J. 1990, *ApJL*, 352, L1
- Rand, R. J. 1997, *ApJ*, 474, 129
- Rand, R. J. 2000, *ApJ*, 537, L13
- Relaño, M., Lisenfeld, U., et al. 2007, *ApJL*, 667, L141
- Reynolds, R. J. 1971, PhD Thesis (The University of Wisconsin - Madison)
- Reynolds, R. J., Scherb, F. & Roesler, F. L. 1973, *ApJ*, 185, 869
- Reynolds, R. J., Haffner, L. M., & Tuft, S. L. 1999, in *New Perspectives on the Interstellar Medium*, ed. A. R. Taylor, T. L. Landecker, & G. Joncas, *ASP Conf. Ser.*, 168, 149
- Rosado, M., Gabbasov, R. F., Repetto, P., et al. 2013, *AJ*, 145, 135
- Rossa, J. & Dettmar, R.-J. 2003, *A&A*, 406, 493
- Rossa, J., Dettmar, R.-J., Waltherbos, R. A. M., & Norman, C. A. 2004, *AJ*, 128, 674
- Sanchez, S. F.; Garcia-Benito, R.; Zibetti, S. et al. 2016, *arxiv:160402289S*
- Shapiro, P. R. & Field, G. B. 1976, *ApJ*, 205, 762
- Shull, M.J., Jones, J.R., Danforth, C.W., & Collins, J.A. 2009, *ApJ*, 699,754, 2009
- Smee, S. A., Gunn, J. E., Uomoto, A. et al. 2013, *AJ*, 146, 32
- Swaters, R. A., Sancisi, R., & van der Hulst, J. M. 1997, *ApJ*, 491, 140
- Wright, E. L., Eisenhardt, P. R. M., Mainzer, A. K. et al. 2010, *AJ*, 140, 1868
- Wu, C. J., Waltherbos, R. A., Rand, R. J. et al. *American Astronomical Society, AAS Meeting 223*, 453.19
- Xilouris, E. M., Byun, Y. I., Kylafis, N. D., et al. 1999, *A&A*, 344, 868
- Yan, Renbin; Tremonti, Christy; Bershady, Matthew A. et al. 2016, 151, 8
- Yoachim, P. & Dalcanton, J. J. 2006, *AJ*, 131, 226
- Zhu, Y.-N., Wu, H., Cao, C., & Li, H.-N., 2008, *ApJ*, 686, 155
- Zschaechner, L. K. & Rand, R. J. 2015, *ApJ*, 808, 153

Zschaechner, L. K., Rand, R. J., Heald, G. H., et al. 2011, ApJ, 740, 35

Zschaechner, L. K., Rand, R. J., Waltherbos, R. A. M., 2015, ApJ799, 61

MANGA-ID	RA(J2000) deg	Dec(J2000) deg	Lag km s <sup>-1</sup> kpc <sup>-1</sup>	e(Lag) km s <sup>-1</sup> kpc <sup>-1</sup>	$z_0(H\alpha)$ kpc	$h(H\alpha)$ kpc	log L(H $\alpha$ )/L $_{\odot}$ dex
1-339166	116.389689	45.772328	28	8	1.3	2.5	6.1
1-43672	116.787163	42.078716	16	7	1.0	3.0	5.9
1-339138 <sup>1</sup>	117.318153	46.205040	11	6	0.9	1.9	6.4
1-44117	118.863856	44.029330	13	6	1.2	4.2	5.9
1-44479	119.822532	42.008537	34	9	1.5	1.5	6.3
1-605549	134.284434	51.471546	4	6	1.0	6.1	5.4
1-216973	135.833415	40.464713	27	8	2.8	6.4	6.5
1-137844	139.427012	44.100687	48	11	1.4	5.4	5.6
1-138034	144.846118	47.126864	35	9	0.9	2.8	6.3
1-275456	159.382717	43.653764	14	6	1.3	1.6	6.2
1-487452	166.631358	22.777630	40	10	0.8	1.2	6.1
1-282144	184.592510	46.155351	11	6	1.8	8.8	6.7
1-258777	186.394835	45.431737	22	7	1.1	3.5	6.4
1-258988	187.722485	45.219432	12	6	2.1	3.4	6.7
1-284197	194.885392	42.758926	17	7	1.2	3.3	5.8
1-591474	197.580687	47.124056	14	6	1.2	2.5	6.1
1-285031	198.701372	47.351547	33	9	1.0	3.0	6.5
1-320642	214.375198	47.714958	9	6	1.1	4.8	6.2
1-134848	244.331994	43.479672	12	6	2.3	7.3	6.8
1-633994	247.419951	40.686954	22	7	1.4	11.0	5.9
1-594602	249.471810	39.249823	54	12	1.8	10.0	6.1
1-95111	250.668078	40.169087	29	8	1.4	6.0	6.1
1-561039 <sup>1</sup>	258.271095	35.268616	24	8	0.7	1.0	5.8
1-23891	260.228215	57.097956	38	10	0.9	4.5	5.6
1-114334 <sup>1</sup>	324.259708	11.906203	73	16	0.7	4.3	5.8

**Table 1.** The rotation velocity lag and parameters of our MaNGA galaxies subsample: MaNGA ID, equatorial coordinates, lag amplitude and its uncertainty, the vertical and radial scales determined from the  $H\alpha$  images, and the total  $H\alpha$  luminosity.

<sup>1</sup> - three galaxies with inclination angles less than  $85^\circ$  are excluded from the figures with the lag in this paper, see text.